

Relativistic vs. Non-relativistic Nuclear Models

Haruki KURASAWA

Department of Physics, Faculty of Science, Chiba University,
Chiba 263-8522, Japan

Tel +81-43-290-3687

Fax +81-43-290-3691

kurasawa@c.chiba-u.ac.jp

Toshio SUZUKI

Department of Applied Physics, Fukui University, Fukui 910-8507, Japan
and

RIKEN, 2-1 Hirosawa, Wako-shi, Saitama 351-0198, Japan

Tel +81-776-27-8780

Fax +81-776-27-8494

suzuki@quantum.apphy.fukui-u.ac.jp

Abstract

Both the relativistic and non-relativistic model explain very well low-energy nuclear phenomena, but in a physically different way from each other. There seems to be no low-energy phenomenon to answer which model is more reasonable. In order to explore a difference between two models, high momentum transfer phenomena are investigated. First it is shown that the neutron spin-orbit charge density in the relativistic model reproduces very well experimental data on elastic electron scattering which have not been explained in the non-relativistic model. Next it is predicted that the relativistic Coulomb sum value is strongly quenched, compared with the non-relativistic one. This quenching is owing to the anti-nucleon degrees of freedom, which make the nucleon size larger and equivalently the vector-meson mass smaller in nuclear medium. New experiment on the Coulomb sum values around the momentum transfer 1GeV is expected to distinguish the relativistic from the non-relativistic model.

[relativistic models vs. non-relativistic models, nuclear structure, electron scattering, Coulomb sum rule]

1 Introduction

There are two kinds of nuclear models which have been extensively studied in recent years. The one is a non-relativistic model which assumes Skyrme forces[1], and the other is a relativistic model which takes into account meson exchanges explicitly[2]. Both models work very well phenomenologically in reproducing the nuclear ground state and low-lying excited states including giant resonances. The problem, however, is that the relationship is not clear between the non-relativistic and relativistic model. The former cannot be obtained in a simple non-relativistic reduction of the latter, or the latter is not a simple relativistic extension of the former. In the relativistic model the effective nucleon-mass coming from the Lorentz-scalar potential and anti-nucleon degrees of freedom play an essential role even in low-energy phenomena, while in the non-relativistic model many-body correlations are necessary. These models now understand nuclear structure in different ways from each other, as briefly reviewed in the next section.

At present there seems to be no low-energy phenomenon to distinguish the one from the other model. In this paper, however, we would like to point out that the relativistic effects hidden in low-energy phenomena manifest themselves in high-energy phenomena in a way peculiar to the relativistic model. Since, if the relativistic model is realistic, high-energy phenomena should be also described within the same framework, such phenomena have a possibility to distinguish the relativistic model from the non-relativistic model.

We will show in the third section that the relativistic model provides us with a peculiar time-component of the nuclear four-current. The neutron spin-orbit charge density is enhanced by the Lorentz scalar potential. As a result, the difference between cross sections for ^{40}Ca and ^{48}Ca is well reproduced, which has not been explained for long time in non-relativistic models.

In the fourth section, we will show how effects of the anti-nucleon degrees of freedom appear in high-momentum transfer reaction. In the relativistic model, the anti-nucleon degrees of freedom are necessary for describing correctly the convection current, the center of mass motion, and giant resonances, but they do not change non-relativistic results at all. In the same framework as for those low-momentum transfer phenomena, we will show that the Coulomb sum values at the high-momentum transfer are strongly quenched owing to the anti-nucleon degrees of freedom. This quenching is

due to the fact that in the relativistic model, the nucleon size is increased and equivalently the vector-meson mass is decreased owing to the presence of the Lorentz scalar potential in nuclear medium.

The final section will be devoted to a brief conclusion.

2 Relativistic vs. Non-relativistic Model

In this section, we briefly review how the relativistic and non-relativistic model explain low-energy nuclear phenomena in different ways from each other. As examples, let us quote the binding energy and giant monopole states.

2.1 Binding Energy

The one of the Skyrme forces in the non-relativistic model yields the the nucleon binding energy in nuclear matter as[1]

$$\frac{E_N}{A} = \frac{k_F^2}{2M} + \left(\frac{3}{4} + \frac{3}{16} t_3 \rho \right) + \frac{1}{10} (3t_1 + 5t_2) \rho k_F^2, \quad (1)$$

where k_F and ρ denote the Fermi momentum and the nucleon density, and t_0, t_1, t_2 and t_3 stand for the parameters in the Skyrme force. The repulsive t_3 -force is necessary for the non-relativistic model in order to prevent the nucleus from the collapse, and is considered to simulate many-body correlations. On the other hand, the simple relativistic model gives the binding energy as[2]

$$\frac{E_R}{A} = \frac{1}{\rho} \left\{ \frac{1}{(2\pi)^3} \int_0^{k_F} dk^3 (\vec{k}^2 + M^{*2})^{1/2} + \frac{1}{2} \left(\frac{m_s}{g_s} \right)^2 U_s^2 + \frac{1}{2} \left(\frac{m_v}{g_v} \right)^2 U_0^2 \right\}, \quad (2)$$

where U_s and U_0 represent the Lorentz-scalar and -vector potential given by the Lorentz-scalar and -vector density as

$$U_s = \left(\frac{g_s}{m_s} \right)^2 \rho_s, \quad U_v = \left(\frac{g_v}{m_v} \right)^2 \rho, \quad (3)$$

$m_{s(v)}$ and $g_{s(v)}$ being the Lorentz-scalar(vector) meson mass and Yukawa coupling constant. The effective mass in Eq.(2) comes from the Lorentz-scalar potential,

$$M^* = M - U_s. \quad (4)$$

As seen in Eq.(2), the higher-order density dependence of the binding energy comes from the relativistic effects, in contrast to the one in the non-relativistic model. The Lorentz scalar potential which yields the effective mass prevents the nucleus from the collapse.

2.2 Giant Monopole States

An important ingredient of the relativistic model is anti-nucleon degrees of freedom. They are necessary even for low-energy phenomena. For example, the excitation energy of the giant monopole state is described in terms of the Landau parameters as in non-relativistic models[3],

$$\omega_0 = \frac{1}{\epsilon_F} \left\{ \frac{3k_F^2}{\langle r^2 \rangle} \frac{1 + F_0}{1 + \frac{1}{3}F_1} \right\}^{1/2}, \quad (5)$$

where F_0 and F_1 denote the Landau parameters, and ϵ_F the Fermi energy. In the relativistic model, the anti-nucleon degrees of freedom are hidden in the Landau parameters. In the $\sigma - \omega$ model, they are described as[4]

$$F_0 = F_v - \frac{1 - v_F^2}{1 + a} F_s, \quad F_1 = -\frac{v_F^2 F_v}{1 + \frac{1}{3}v_F^2 F_v}, \quad (6)$$

where we have defined

$$\begin{aligned} F_s &= N_F \left(\frac{g_s}{m_s} \right)^2, \quad F_v = N_F \left(\frac{g_v}{m_v} \right)^2, \quad N_F = \frac{2k_F E_F}{\pi^2}, \quad E_F = \{k_F^2 + M^{*2}\}^{1/2}, \\ v_F &= k_F/E_F, \quad a = \frac{3}{2} \left(1 - \frac{2}{3}v_F^2 + \frac{1 - v_F^2}{2v_F} \ln \frac{1 - v_F}{1 + v_F} \right). \end{aligned}$$

It has been shown that the denominators of Eq.(6) come from nucleon-antinucleon excitations in the configuration space of RPA[5]. The similar role of the anti-nucleon in the relativistic model can be found in excitation energies of other giant resonances and the nuclear convection current or magnetic moments[6, 7]. In particular, the continuity equation is not satisfied without nucleon-antinucleon excitations[5].

Thus, in the relativistic model, the anti-nucleon degrees of freedom are necessary even for low-energy phenomena, but we cannot distinguish it from the non-relativistic model by these phenomena, since there is no difference between their relativistic and non-relativistic expressions, as in Eq(5).

We note that in Eq.(6) the relativistic effects are also important. If the effects of $O(v_F^2)$ are neglected, we have $F_0 < -1$ which implies the nuclear collapse. Furthermore, we have $F_1 = 0$. It comes from the space part of the ω -meson exchange which is usually neglected in the non-relativistic model.

3 Elastic Electron Scattering

Now let us discuss high momentum transfer phenomena where relativistic effects are expected to appear. Of course non-relativistic models do not contain such effects. Hence, we must find relativistic effects which are not a simple correction to non-relativistic models, but are peculiar to the present relativistic model.

First we discuss elastic electron scattering from nuclei. In order to calculate the cross section in phase-shift analyses, we need the nuclear charge density,

$$\rho_c(r) = \int \frac{d^3q}{(2\pi)^3} \exp(-i\vec{q} \cdot \vec{r}) \langle 0 | \hat{\rho}(\vec{q}) | 0 \rangle \quad (7)$$

where the time-component of the relativistic nuclear-four current is given by

$$\langle 0 | \hat{\rho}(\vec{q}) | 0 \rangle = \langle 0 | \sum_k \exp(i\vec{q} \cdot \vec{r}_k) \left(F_{1k}(\vec{q}^2) + \frac{\mu_k}{2M} F_{2k}(\vec{q}^2) \vec{q} \cdot \vec{\gamma}_k \right) | 0 \rangle. \quad (8)$$

Using the Sachs form factor instead of the Dirac form factor $F_1(\vec{q}^2)$, it is rewritten as

$$\langle 0 | \hat{\rho}(\vec{q}) | 0 \rangle = \int d^3x \exp(i\vec{q} \cdot \vec{x}) \sum_{\tau} \left(G_{E\tau}(\vec{q}^2) \rho_{\tau}(x) + F_{2\tau}(\vec{q}^2) W_{\tau}(x) \right), \quad (9)$$

where τ denotes the proton and neutron. The nucleon density $\rho_{\tau}(r)$ and the spin-orbit density $W_{\tau}(r)$ in the above equation are given in the relativistic model as

$$\rho_{\tau}(r) = \sum_{\alpha} \frac{2j_{\alpha} + 1}{4\pi r^2} \left(G_{\alpha}^2 + F_{\alpha}^2 \right), \quad (10)$$

$$W_{\tau}(r) = \frac{\mu_{\tau}}{M} \sum_{\alpha} \frac{2j_{\alpha} + 1}{4\pi r^2} \times \frac{d}{dr} \left(\frac{M - M^*(r)}{M} G_{\alpha} F_{\alpha} + \frac{\kappa_{\alpha} + 1}{2Mr} G_{\alpha}^2 - \frac{\kappa_{\alpha} - 1}{2Mr} F_{\alpha}^2 \right), \quad (11)$$

where

$$\mu_p = 1.793, \quad \mu_n = -1.913, \quad \kappa_\alpha = (-1)^{j-\ell+1/2}(j + 1/2).$$

In the non-relativistic model, we have the only large component G_α , but no small component F_α of the single-particle wave function. As a result, there is no spin-orbit density in the non-relativistic model, since it is in order of $1/M^2$, while Schrödinger equation is in order of $1/M$. In the relativistic model, on the other hand, we have the spin-orbit density coming from both protons and neutrons. In the present relativistic model, it is enhanced by the effective mass. The enhancement is more clearly seen in the Fourier transform of Eq.(11):

$$W_\tau(q) \approx \frac{\mu_\tau}{M} q \sum_\alpha (2j_\alpha + 1) \int_0^\infty dr \frac{\kappa_\alpha + 1}{2M_* r} G_\alpha^2 j_1(qr), \quad (12)$$

where we have defined

$$2M_*(r) = E + M^*(r) - U_0(r) \approx 2M^*(r). \quad (13)$$

This spin-orbit density is not negligible, in particular, in neutron-rich nuclei where the subshell is not occupied by the protons.

An example[8] is shown in Fig. 1 which shows the elastic-scattering cross sections for ^{40}Ca and ^{48}Ca on the top and their difference $D(\theta)$ on the bottom as a function of the electron-scattering angle in the case of the incident energy 249.5 MeV. The solid curves on the l.h.s. of Fig.1 are obtained in the non-relativistic model using the SLy4 force[1]. We clearly see a disagreement with experiment[9] on the difference between the two cross sections. Other Skyrme forces available at present yield similar results for the difference. We note that the neutron charge densities are taken into account properly in these non-relativistic calculations, although their contribution to the cross sections are negligible. On the other hand, the solid curves of the r.h.s. of Fig. 1 are obtained in the relativistic model with NL-SH parameter set[10]. The thick and thin solid curves are calculated with and without the spin-orbit density, respectively. In ^{40}Ca , the two curves coincide with each other, since the spin-orbit density has almost no effects in doubly closed shell nuclei. It is seen that the difference between the cross sections for ^{40}Ca and ^{48}Ca is well reproduced in the relativistic model owing to the neutron spin-orbit density peculiar to the relativistic model. If electron scattering off unstable nuclei becomes available in the near future, we expect that the difference between the relativistic and non-relativistic models would be explored in more detail.

4 Quasielastic Scattering

In the low-energy phenomena mentioned in the subsection 2.2, we cannot see effects of the anti-nucleon degrees of freedom explicitly, since they do not change the results of the non-relativistic model at all. We notice, however, that those phenomena are all related to the zero limit of the momentum transfer q in the RPA response functions[5]. At the finite momentum transfer, effects of the nucleon-antinucleon excitations appear in the RPA response function. This fact has been shown in the longitudinal response function for quasielastic scattering[11, 12]. The response function is strongly quenched by the effects of order \vec{q}^2 as discussed below.

Fig. 2 shows the Coulomb sum values as function of the momentum transfer. The dashed and solid curves show the results of the relativistic RPA without and with the nucleon-antinucleon excitations, respectively. The non-relativistic results are similar to the dashed one. It is seen that above the momentum transfer 0.5 GeV, the Coulomb sum values are strongly quenched due to the nucleon-antinucleon excitations.

The reason why the Coulomb sum values are quenched is easily understood in Fig. 3. The Dirac form factor F_1 in the free space includes the second diagram of the r.h.s. in which the nucleon-antinucleon excitations participate with the free mass M . In nuclear medium, however, nucleons and anti-nucleons have the effective mass $M^* = M - U_s$ in the relativistic model. This effective mass modifies the Dirac form factor, that is the proton radius. Using the RPA correlation function, the modification of the proton size is estimated as[13]

$$\langle r_p^2 \rangle^* = \langle r_p^2 \rangle + \delta \langle r_p^2 \rangle, \quad \delta \langle r_p^2 \rangle \approx \frac{1}{\pi^2} \left(\frac{g_v}{m_v} \right)^2 \ln \left(\frac{M}{M^*} \right). \quad (14)$$

Since $M > M^*$ due to the Lorentz scalar potential, we have always $\delta \langle r_p^2 \rangle > 0$ in the relativistic model. In the present calculation, we have determined the coupling constants so as to reproduce the nucleon binding energy and nuclear density of nuclear matter. Then, we obtain

$$\left(\frac{\langle r_p^2 \rangle^*}{\langle r_p^2 \rangle} \right)^{1/2} = 1.146, \quad (M^* = 0.731M). \quad (15)$$

Thus, since the effective nucleon mass is smaller in the nuclear medium, the proton size is increased. This means that the nucleon form factor is reduced.

This is the reason why the Coulomb sum values are strongly quenched due to the anti-nucleon degrees of freedom. We note that if we define the effective ω -meson mass m_v^* by its RPA self-energy, Eq.(14) is expressed as[12]

$$\delta\langle r_p^2 \rangle \approx 3 \left(\frac{1}{m_v^{*2}} - \frac{1}{m_v^2} \right), \quad (16)$$

as expected in the vector-meson dominance model. The quenching of the Coulomb sum is also interpreted as the reduction of the ω -meson mass in nuclear medium, which is $m_v^* = 0.696m_v$ in the present model.

In Fig. 2 experimental data are shown from Saclay[14] and SLAC[15] which seem to support the quenching, but there are discussions on their analyses of the data[16, 17]. The prediction of the relativistic model should be examined in more detail with new experiment.

Finally we should mention that the modified nucleon form factor slightly improves also an agreement of elastic-scattering cross section with experiment. In Fig. 4 is shown the result of NL-SH for the nucleon form factor corresponding to the radius Eq.(15) with the same designation as in Fig.1.

5 Conclusions

The relativistic and non-relativistic model work well for low-energy nuclear phenomena, but explain them in different ways from each other. In high momentum transfer phenomena, however, there is a difference between their predictions. The relativistic effects in the relativistic model are not obtained as a simple correction to the non-relativistic models.

First we have shown that the relativistic model reproduces the difference between the cross sections for elastic electron scattering from ^{40}Ca and ^{48}Ca , which has not been explained in non-relativistic models. The time-component of the relativistic four-current includes the neutron spin-orbit current which is enhanced by the Lorentz scalar potential. Electron scattering off unstable nuclei may be useful for distinguishing the relativistic from the non-relativistic model in more detail.

Second, we have shown a role of the anti-nucleon degrees of freedom. They are required from the fundamental reason in the relativistic model, but they are hidden in low-energy phenomena. Within the same framework for the low-energy phenomena, however, it is shown that effects of the anti-nucleons with the effective mass appear in the Coulomb sum rule at high-momentum

transfer. Since the anti-nucleon degrees of freedom are an important ingredient of the relativistic model, observation of those effects is essential for the question if the relativistic model is realistic. New experiment on the Coulomb sum values around the momentum transfer 1 GeV is desirable in order to answer this question. It would be very serious for the relativistic model, if the Coulomb sum values are not quenched, compared with the non-relativistic one.

References

- [1] E. Chabanat et al., Nucl. Phys. A635, 231 (1998).
- [2] B. Serot and J. Walecka, Adv. Nucl. Phys. 16, 1(1986).
- [3] S. Nishizaki, H. Kurasawa and T. Suzuki, Nucl. Phys. A462, 687 (1987).
- [4] H. Kurasawa and T. Suzuki, Nucl. Phys. A454, 527 (1986).
- [5] H. Kurasawa and T. Suzuki, Phys. Lett. B474, 262 (2000); Z. Ma et al., Nucl. Phys. A686, 173 (2001)
- [6] H. Kurasawa and T. Suzuki, Phys. Lett. 165B, 234 (1985).
- [7] W. Bentz W. et al., Nucl. Phys. A436, 593 (1985).
- [8] H. Kurasawa and T. Suzuki, Phys. Rev. C62, 054303 (2000).
- [9] R. Frosch et al., Phys. Rev. 174, 1380 (1968).
- [10] M. Sharma et al., Phys. Lett. B312, 377 (1993).
- [11] H. Kurasawa and T. Suzuki, Nucl. Phys. A490, 571 (1988).
- [12] H. Kurasawa and T. Suzuki, Prog. Theor. Phys. 86, 773 (1991).
- [13] H. Kurasawa and T. Suzuki, Phys. Lett. B208, 160; B211, 500 (1988).
- [14] Z. -E. Meziani et al., Phys. Rev. Lett. 54, 1233 (1985).
- [15] J. Chen, Phys. Rev. Lett. 66, 1283 (1991).
- [16] J. Jourdan, Phys. Lett. B353, 189 (1995); Nucl. Phys. A603, 117 (1996).
- [17] J. Morgenstern and Z. -E. Meziani, to be published in Phys. Lett. B.

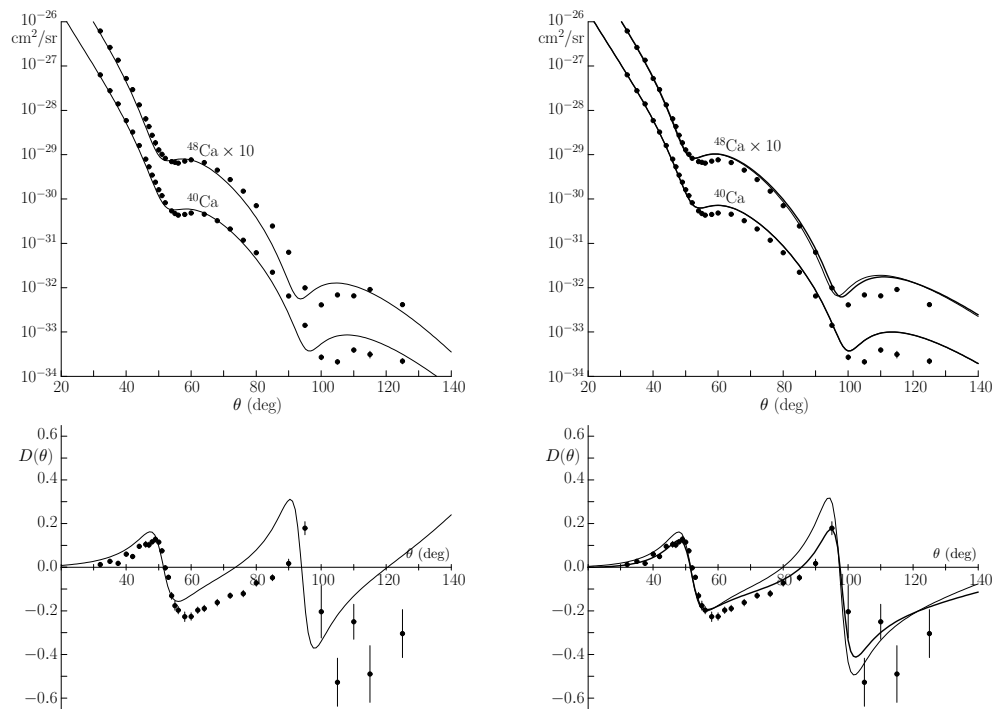


Figure 1: Elastic-scattering cross sections for ^{40}Ca and ^{48}Ca and their difference. For the details, see the text.

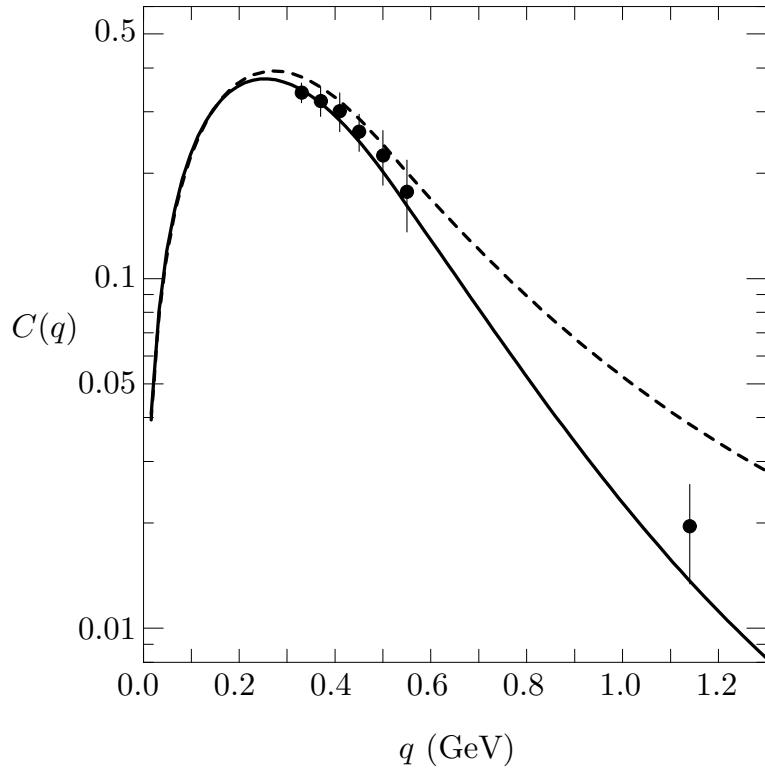


Figure 2: The Coulomb sum values as a function of the momentum transfer. For the details, see the text.

$$F_1 \gamma_\mu \blacksquare \text{ wavy} = \gamma_\mu \bullet \text{ wavy} + \gamma_\mu \bullet \text{---} \omega \text{---} \text{N} \text{---} \overline{\text{N}} \text{---} \text{wavy}$$

Figure 3: Dirac form factor.

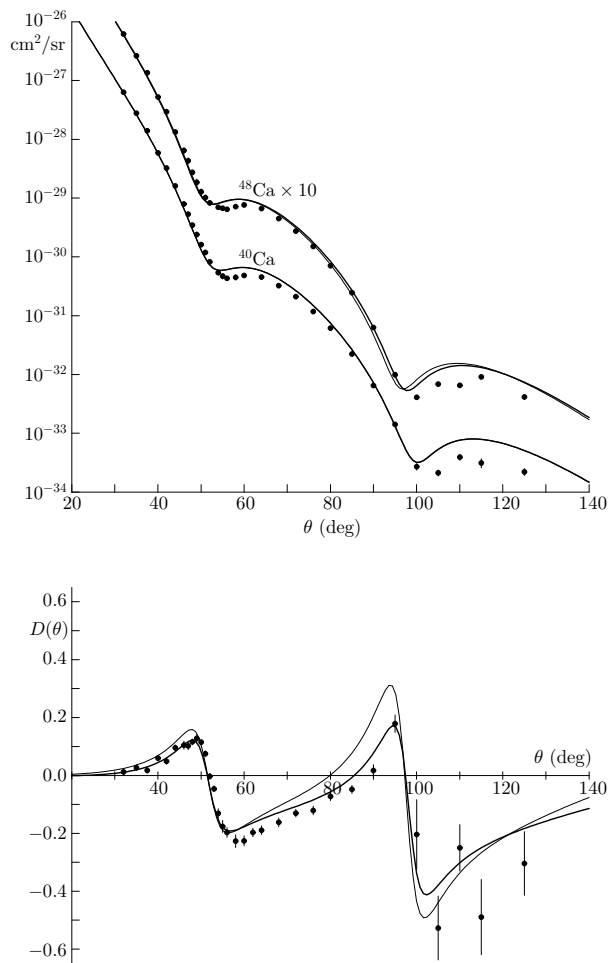


Figure 4: Same as Fig. 1, for NL-SH with the nucleon form factor corresponding to the radius Eq.(15)